Glycoproteomics characterization of immunoglobulins in health and disease

Plomp, H.R.

Citation

Plomp, H. R. (2017, May 31). *Glycoproteomics characterization of immunoglobulins in health and disease*. Retrieved from https://hdl.handle.net/1887/49752

Cover Page

Universiteit Leiden

Author: Plomp, H.R.
Title: Glycoproteomics characterization of immunoglobulins in health and disease
Issue Date: 2017-05-31

Chapter 2:

Site-specific *N*-Glycosylation analysis of human immunoglobulin E

Authors: Rosina Plomp[1], Paul J. Hensbergen[1], Yoann Rombouts[1,2,3], Gerhild Zauner[1,4], Irina Dragan[1], Carolien A. M. Koeleman[1], André M. Deelder[1], Manfred Wuhrer[1]

[1]*Center for Proteomics and Metabolomics, Leiden University Medical Center, Leiden, The Netherlands;*
[2]*Department of Rheumatology, Leiden University Medical Center, Leiden, The Netherlands;*
[3]*present address: Institut de Pharmacologie et de Biologie Structurale, Université de Toulouse, CNRS, UPS, France;*
[4]*present address: Imperial Innovations, London, the United Kingdom*

Table of Contents

2.1: Summary

Immunoglobulin E (IgE) is a heterodimeric glycoprotein involved in anti-parasitic and allergic immune reactions. IgE glycosylation is known to exhibit significant inter-individual variation, and several reports have indicated its relevance in determining IgE activity. Here, we present site-specific glycosylation analysis of IgE from three different sources: IgE from the serum of a hyperimmune donor, from the pooled serum of multiple non-diseased donors, and from the pooled serum of 2 patients with IgE myeloma. The heavy chains were isolated and digested with either trypsin, proteinase K or chymotrypsin, which permitted coverage of all seven potential *N*-glycosylation sites. The resulting (glyco-)peptides were analyzed by nano-reverse phase-LC-MS/MS and MALDI-TOF/TOF-MS/MS. Site Asn264 was shown to be unoccupied. In all three samples, site Asn275 contained exclusively oligomannosidic structures with between 2 and 9 mannoses, while sites Asn21, Asn49, Asn99, Asn146 and Asn252 contained exclusively complex-type glycans. For the non-myeloma IgE, the majority of these glycans were biantennary, core-fucosylated and contained one or two terminal *N*-acetylneuraminic acids. In contrast, myeloma IgE showed a higher abundance of triantennary and tetraantennary glycan structures, and a low abundance of species with a bisecting *N*-acetylglucosamine. Our approach allows comparison of the glycosylation of IgE samples in a site-specific manner.

2.2: Introduction

Immunoglobulin E (IgE) is the least abundant of the immunoglobulins in human blood, present at an average concentration of approx. 150-300 ng/ml in serum (1-3). It exists in both a soluble form and as a membrane-bound receptor. Like several other immunoglobulins, IgE consists of two heavy and two light chains, with the variable regions of both chains together forming the antigen binding site. In contrast to other members of the immunoglobulin family, which contain a hinge region, IgE adopts a more rigid, asymmetrically bent conformation (4). IgE is involved in anti-parasitic immune reactions (5), but is mostly known for its role in allergic responses (6). Allergic responses originate when allergen-bound IgE triggers mast cell and basophil degranulation, thereby releasing pro-inflammatory mediators. Furthermore, IgE serum levels have been found to be elevated in individuals with allergies (3).

Roughly 12% of the molecular mass of IgE can be attributed to oligosaccharides, making it the most heavily glycosylated immunoglobulin (7). The biological function of IgE glycosylation is still largely unclear. While glycosylation is essential for the secretion of IgE, further processing of the precursor glycans ($Glc_3Man_9GlcNAc_2$) is not required for secretion, allergen binding or mast cell activation (8). Several IgE Fc receptors have been described. The high affinity IgE receptor FcεRI is expressed on the surface of basophils and mast cells, and is preloaded with IgE under physiological conditions (9). When antigen binds to IgE and crosslinks the receptors, this triggers the release of histamine and other pro-inflammatory mediators from the cells. While a severe loss in binding between IgE and FcεRI after glycan release has been described (10), others observed that glycosylation appears to account for only a minor or no contribution to receptor binding (11-13). CD23, also known as the low affinity IgE receptor FcεRII, is present on the surface of various immune cells, as well as in a soluble form in serum (6). Glycosylation of IgE does not appear to be required for IgE-CD23 binding, but it has been shown to shield IgE from interacting with CD23, as evidenced by an increase in binding affinity observed after enzymatic deglycosylation of myeloma-derived IgE (13). In addition to the Fc-receptors, several galectins have been shown to interact with IgE in a glycosylation-dependent manner. Galectin-3, formerly known as IgE-binding protein, is a secretory protein which can bind to both IgE and FcεRI (14). It is thought to trigger mast cell degranulation by crosslinking IgE and/or FcεRI (14). Galectin-9, a lectin known to suppress mast cell degranulation, also binds to IgE (15).

Human IgE possesses 7 potential *N*-glycosylation sites within the conserved region of the heavy chain. In studies performed on myeloma-derived IgE and on recombinant IgE, six of these sites were found to be occupied (7, 16-18). No *N*-glycans were attributed to site Asn264. Asn275 was found to contain solely oligomannosidic glycans, while the remaining 5 sites were reported to be occupied by complex-type glycan structures (7, 17-19). The presence of a majority (85%) of complex and a minority (14%) of oligomannosidic glycans was confirmed for non-myeloma IgE by Arnold *et al*. using IgE from a single hyperimmune donor (20). Over 20 different kinds of released oligosaccharides were identified in this study. Oligomannosidic glycans were found to carry between 4 and 8 mannose residues, while complex-type glycans appeared to be largely biantennary (97%), core-fucosylated (68%), containing 1 or 2 terminal *N*-acetylneuraminic acids (88%), with a minority (15%) containing a bisecting GlcNAc residue (an *N*-acetylglucosamine β1-4-linked to the innermost mannose) (20). Most studies on IgE have been performed using monoclonal myeloma-derived IgE, which probably does not resemble overall serum IgE glycosylation. In addition, it is known that inter-individual differences are present in the glycosylation of IgE, although this has not been explored using site-specific glycosylation analysis (21). Hence, studies on IgE glycosylation from different sources, resembling different (patho)physiological conditions, preferably in a site-specific manner, are needed.

To this end, an in-depth glycoproteomics analysis of polyclonal IgE is required and the aim of the current study was to develop such a method. IgE heavy chains from different sources (control, hyperimmune and myeloma) were digested using either trypsin, proteinase K or chymotrypsin. Resulting (glyco-)peptides, covering all 7 potential *N*-glycosylation sites, were analyzed by nano-reverse phase (RP)-LC-ESI-ion trap (IT)-MS/MS and MALDI-TOF/TOF-MS/MS. These techniques have been shown to be well suited for glycopeptide detection and characterization (22-24). From these spectra, the *N*-glycans present at each site were inferred, and a site-specific glycosylation profile was established for each of the three types of IgE.

2.3: Methods

2.3.1: IgE sources

Polyclonal IgE was acquired from 3 commercial sources. IgE from Athens Laboratories (Athens, GA) was derived from the serum of a single donor with a hyperimmune condition. IgE from US Biological (Swampscott, MA) was isolated from the pooled serum of non-diseased donors. IgE from Scripps Laboratories (San Diego, CA) was purified from the pooled serum of two IgE myeloma (kappa and lambda) patients.

2.3.2: SDS-PAGE and in-gel enzymatic digestion

Five µg of IgE was reduced with 2-mercaptoethanol (Sigma-Aldrich, St. Louis, MO) at 95°C for 10 min and analyzed by SDS-PAGE on a NuPage 4-12% gradient Bis-Tris gel (Life Technologies, Carlsbad, CA) using NuPage MES SDS running buffer (Life Technologies). The gel was stained with Coomassie G-250 (SimplyBlue SafeStain, Life Technologies). The bands containing the heavy chain (at approx. 75 kDa) and the light chain (at approx. 27 kDa) were excised and cut into pieces. The gel pieces were washed with 25 mM ammonium bicarbonate (Sigma-Aldrich) and dehydrated with acetonitrile (ACN) (Biosolve, Valkenswaard, the Netherlands). The proteins were then reduced in-gel for 30 min at 56°C with 50 µl of a 10 mM DL-dithiothreitol (DTT) (Sigma-Aldrich) 25 mM ammonium bicarbonate solution, followed by dehydration of the gel pieces in ACN and cysteine alkylation for 20 min with 50 µl of a 55 mM iodoacetamide (Sigma-Aldrich) 25 mM ammonium bicarbonate solution in the dark. The gel pieces were subsequently incubated in 25 mM ammonium bicarbonate, followed by removal of the solution and incubation in ACN. This was repeated once, and the gel pieces were subsequently dried in a centrifugal vacuum concentrator (Eppendorf, Hamburg, Germany) at 30°C for 5 min.

Proteolytic digestion was performed by adding 30 µl of 25 mM ammonium bicarbonate containing either 0.15 µg trypsin (sequencing grade modified trypsin, Promega, Madison, WI), 1 µg proteinase K (from *Tritirachium album*, Sigma-Aldrich) or 0.25 µg chymotrypsin (sequencing grade from bovine pancreas, Roche Applied Sciences, Penzberg, Germany) to the dried gel particles. The samples were kept on ice for 1 h to observe whether the gel pieces were fully submerged (10 µl 25 mM ammonium bicarbonate was added if this was not the case) and were subsequently incubated overnight at 37°C. The solution surrounding the gel pieces was collected and stored at -20°C. We then added 20 µl of 25 mM ammonium

bicarbonate to the gel pieces, and incubation was continued at 37°C degrees for another hour. The solution was again collected and added to the first fraction prior to freezing.

In order to identify the amino acid sequence of the peptide moiety of glycopeptides, several samples were deglycosylated with *N*-glycosidase F (*N*-glycosidase F of *Flavobacterium meningosepticum*, Roche Applied Sciences), either in-gel (before the addition of a proteolytic enzyme) or in-solution (after in-gel proteolytic digestion had already taken place). For in-gel deglycosylation, the same digestion protocol as described above was implemented, but instead of a proteolytic enzyme, 0.04 μg (1 unit) of *N*-glycosidase F in 30 μl 25 mM ammonium bicarbonate was added to the dried gel particles. After overnight incubation at 37°C, the solution surrounding the gel pieces was discarded, followed by incubation in 25 mM ammonium bicarbonate, dehydration in ACN, drying with a centrifugal vacuum concentrator, and the addition of a proteolytic enzyme. For in-solution deglycosylation, around 1.5 μg of digested IgE and 0.02 μg *N*-glycosidase F (0.5 units) were brought to a total volume of 20 μl with Milli-Q-purified water and incubated overnight at 37°C.

2.3.3: LC-ESI-MS(/MS) and MALDI-TOF-MS(/MS) analysis

(Glyco-)peptides were analyzed by nano-RP-LC-ESI-ion trap-MS(/MS) on an Ultimate 3000 RSLCnano system (Dionex/Thermo Scientific, Sunnyvale, CA) coupled to an HCTultra-ESI-IT-MS (Bruker Daltonics, Bremen, Germany). Five μl of sample was injected and concentrated on a trap column (Acclaim PepMap100 C18 column, 100 μm x 2 cm, C18 particle size 5 μm, pore size 100 Å, Dionex/Thermo Scientific) before separation on an Acclaim PepMap RSLC nano-column (75 μm x 15 cm, C18 particle size 2 μm, pore size 100 Å, Dionex/Thermo Scientific).

A flow rate of 300 nl/min was applied. Solvent A consisted of 0.1% formic acid in water; solvent B of 0.1% formic acid in 95% ACN and 5% water. A linear gradient was applied with the following conditions: t=0 min, 3% solvent B; t=6 min, 3% solvent B; t=54 min, 40% solvent B; t=64 min, 65% solvent B; t=71 min, 65% solvent B; t=71.5 min, 90% solvent B; t=75 min, 90% solvent B.

Samples were ionized in positive ion mode with an online nanospray source (1000-1300 V) using fused-silica capillaries and a Distal Coated SilicaTip Emitter (New Objective, Woburn,

MA) with an internal diameter of 20 μm (10 μm at the tip) and a length of 5 cm. Solvent evaporation was performed at 170°C with a nitrogen flow of 10 l/min.

For the detection of glycopeptides, the MS ion detection window was set at *m/z* 600-1800 and the MS/MS detection window at *m/z* 140-2200, with automated selection of the 5 highest peaks in the spectrum for MS/MS analysis. Singly charged ions were excluded from fragmentation. For the analysis of *N*-glycosidase F-treated peptide samples, the ion detection window was set at *m/z* 300-1800 for MS and *m/z* 140-2200 for MS/MS.

The amino acid sequence of several glycopeptides could not be identified through LC-MS/MS analysis of N glycosidase F-treated samples. Therefore, MS3 was performed on the original glycopeptide sample. For this, the precursors for both MS2 and MS3 were defined manually in the MS software. In the MS2 fragmentation spectrum of the glycopeptide, the peak corresponding to the peptide with only a single *N*-acetylglucosamine (GlcNAc) or with a GlcNAc and a fucose residue was fragmented, leading to an MS3 spectrum containing b and y ion fragments which allow identification of the amino acid sequence.

In addition, MALDI-TOF-MS and MALDI-TOF/TOF-MS/MS with laser-induced dissociation were performed for peptide analysis on an UltrafleXtreme (Bruker Daltonics) using FlexControl 3.3 software (Bruker Daltonics) in positive ion mode. Proteolytic digests were spotted on an MTP 384 polished steel target plate (Bruker Daltonics) together with 1 μl of 2,5-dihydroxybenzoic acid (DHB) matrix (20 mg/ml in 50% ACN, 50% water). A peptide calibration standard (Bruker Daltonics) was used for external calibration. MALDI-TOF(/TOF)-MS/(MS) data was analyzed with FlexAnalysis (Bruker Daltonics).

2.3.4: Data processing

The LC-MS/MS results were analyzed using DataAnalysis 4.0 software (Bruker Daltonics) and screened manually for the masses of common oxonium fragment ions (*m/z* 366.1: [1 hexose + 1 GlcNAc + H]$^+$; *m/z* 657.2: [1 hexose + 1 GlcNAc + 1 *N*-acetylneuraminic acid + H]$^+$; *m/z* 528.2: [2 hexoses + 1 GlcNAc + H]$^+$), which are characteristic for fragmentation spectra of glycopeptides. Glycopeptide MS/MS spectra were further analyzed manually to derive the oligosaccharide structure and the mass of the peptide moiety, which was then searched against a list of theoretical peptide sequences generated by IgE heavy chain digestion, using the ExPASY FindPept software tool

(http://www.expasy.org/tools/findpept.html). This was done with a mass tolerance of 0.5 Da, the enzyme settings on 'no enzyme', and while selecting the option of iodoacetamide-treated cysteines. The resulting candidate peptide sequences were then confirmed with LC-MS/MS analysis of *N*-glycosidase F-treated samples, using Protein Prospector MS-Product (http://prospector.ucsf.edu/prospector/cgi-bin/msform.cgi?form=msproduct) to calculate expected b and y ion fragmentation peaks.

Mascot generic files (.mgf) were generated with DataAnalysis and analyzed automatically with Mascot Daemon version 2.2.2 (Matrix Science, London, UK). The following conditions were used when operating Mascot Daemon: database: SwissProt; taxonomy: Homo sapiens; enzyme: trypsin/ chymotrypsin/ proteinase K; fixed modifications: carbamidomethyl (C); variable modifications: oxidation (M) (and deamidated (NQ) for *N*-glycosidase F-treated samples); maximal amount of missed cleavages: 1; peptide charge: 2+ and 3+; peptide tolerance MS: 0.6 Da; peptide tolerance MS/MS: 0.4 Da; #13C: 1.

Relative quantification of the glycoforms present at each site was achieved by summing the *m/z* over a fixed time window surrounding the elution time of each glycopeptide, and determining the average background-corrected intensity of the two highest isotope distribution peaks of the glycopeptide in the LC-MS data (if the glycopeptide was present in more than one charge state, the background-corrected intensities of multiple peaks were summed). This value was then normalized against the sum of the intensities of all glycopeptides which contained the same peptide moiety. For some glycopeptide species, modifications of approx. +17.0 Da and -18.0 Da were present, which are expected to be the result of ammonia addition and water loss, respectively. If the intensity of the modified peptide peak exceeded 20% of the intensity of the unmodified peptide peak, the total summed intensity of both peaks was used for relative quantification.

To determine the degree of occupancy of potential *N*-glycosylation sites, LC-MS or MALDI-TOF-MS analysis was performed on an *N*-glycosidase F-treated sample. For peaks belonging to peptides containing a potential *N*-glycosylation site, the isotope distribution was investigated to derive the ratio of the deamidated peptide (with the asparagine amino acid modified to an aspartic acid, increasing the mass by 1 Da and indicating that a glycan structure had been attached prior to deglycosylation) versus the unmodified peptide. This was done by using the theoretical isotope distribution of both peptides as determined by the

Isotope Distribution Calculator (IDCalc) 3.0 (University of Washington, Seattle, Washington). If the deamidated peptide was also found in a non-*N*-glycosidase F-treated sample which was incubated under the same conditions as the treated sample, spontaneous deamidation was determined to be present and a correction was performed to account for this phenomenon.

Additionally, a second method was used to calculate the degree of partial occupation. This involved relative quantification of glycopeptides and the corresponding unoccupied peptide from LC-MS data of a non-deglycosylated sample, by normalizing the background-corrected average intensity of the two highest isotope peaks to the total intensity of both glycopeptides and unoccupied peptide. A correction was applied to account for the difference in isotope distribution between glycopeptides and peptides.

Protein sequence alignment was performed using two different algorithms: Protein BLAST (NCBI) and Clustal Omega (EMBL-EBI), using the default parameters.

2.4: Results

Polyclonal IgE was obtained from three different sources: from the serum of a hyperimmune donor (which will be referred to as hyperimmune-IgE), from the pooled serum of multiple healthy donors (healthy-IgE), and from the pooled serum of two patients with IgE myeloma (myeloma-IgE). All three IgE samples were analyzed by SDS-PAGE, the bands were excised and the extracted *N*-glycopeptides subjected to nano-RP-LC-ESI-IT-MS/MS after tryptic digestion, revealing IgE heavy chains and kappa and lambda light chains (Figure 2.1). While the myeloma-IgE was reportedly derived from the pooled serum of both a donor with kappa-type myeloma as well as a donor with lambda-type myeloma, only the kappa chain was found.
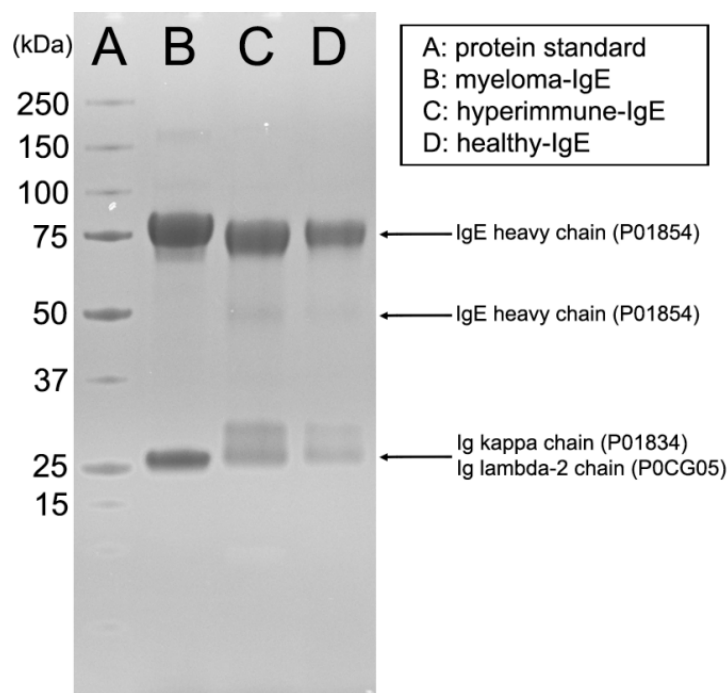

Figure 2.1: SDS-PAGE analysis of IgE derived from the pooled serum of two donors with IgE myeloma (myeloma-IgE), from the serum of a single donor with a hyperimmune condition (hyperimmune-IgE) and from the serum of multiple healthy donors (healthy-IgE). Proteomics analysis of LC-ESI-IT-MS/MS data resulted in the identification of several proteins, of which the most significant are listed with their corresponding primary UniProt accession number. A more comprehensive list of identified proteins can be found in Supplemental Table S2.5.

Hyperimmune-IgE and healthy-IgE displayed a double band containing Ig light chains, while myeloma-IgE showed a single band. Enzymatic deglycosylation of hyperimmune-IgE prior to SDS-PAGE analysis resulted in the appearance of only a single light chain band, indicating that the light chain is present in both a glycosylated and non-glycosylated form in healthy-IgE and hyperimmune-IgE. This was confirmed by LC-ESI-IT-MS/MS analysis of tryptic peptides, which showed that the upper light chain band contained several glycopeptides, whereas none were found in the lower light chain band. Since no consensus *N*-glycosylation site is present in the conserved region of the light chain, we assume that the glycosylation in these samples is present on the variable part of the light chain.

Seven potential *N*-glycosylation sites are present in the constant region of the human IgE heavy chain (Uniprot P01854); Asn21, Asn49 and Asn99 on domain C_H1, Asn146 on C_H2 and Asn252, Asn264 and Asn275 on C_H3. To study site-specific IgE heavy chain glycosylation, in-gel digestions were performed using trypsin, chymotrypsin and proteinase K, and these samples were analyzed by LC-ESI-IT-MS/MS. The LC-MS/MS data was screened for the masses of oxonium fragment ions (*m/z* 366.1: [1 hexose + 1 GlcNAc + H]$^+$; *m/z* 657.2: [1 hexose + 1 GlcNAc + 1 *N*-acetylneuraminic acid + H]$^+$; *m/z* 528.2: [2 hexoses + 1 GlcNAc + H]$^+$), which allowed detection of fragmentation spectra belonging to glycopeptides. Peptide moieties were assigned by matching the peptide mass derived from the fragmentation spectrum (often deduced from the peptide fragment ion with a GlcNAc or a GlcNAc and fucose attached) to theoretical peptide masses from IgE covering the potential *N*-glycosylation sites. In most cases, these peptide moieties were confirmed either by LC-ESI-IT-MS/MS analysis of samples after treatment with *N*-glycosidase F (Supplemental Figure S2.1) or by MS3 experiments. A list of the peptide sequences identified using this methodology is outlined in Supplemental Table S2.1. To exemplify our approach and the different types of glycosylation observed, several MS/MS spectra will be described below.

The fragmentation spectrum in Figure 2.2A shows a proteinase K-generated glycopeptide (*m/z* of 971.36 [M+3H]$^{3+}$) displaying glycan fragments at *m/z* 366.1 and 657.2. Other fragments could be attributed to the glycopeptide after the loss of several sugar residues. Overall this revealed a disialylated, biantennary *N*-glycan structure. While a fragment resembling the peptide moiety is not present, the peptide mass can be deduced from the fragment at *m/z* 764.40 ([M+H]$^+$) corresponding to the peptide with one *N*-acetylglucosamine attached. This peptide mass (561.32 Da, [M+H]$^+$) matches with the peptide TINIT (aa 144-148), containing the *N*-glycosylation site Asn146. This peptide sequence was confirmed by analysis of the deglycosylated sample (Supplemental Table S2.1).

Figure 2.2B shows the fragmentation spectrum of a tryptic glycopeptide covering Asn99 which contains a monosialylated, triantennary glycan moiety. The amino acid sequence was confirmed after analysis of the deglycosylated sample (Supplemental Figure S2.1 and Supplemental Table S2.1).
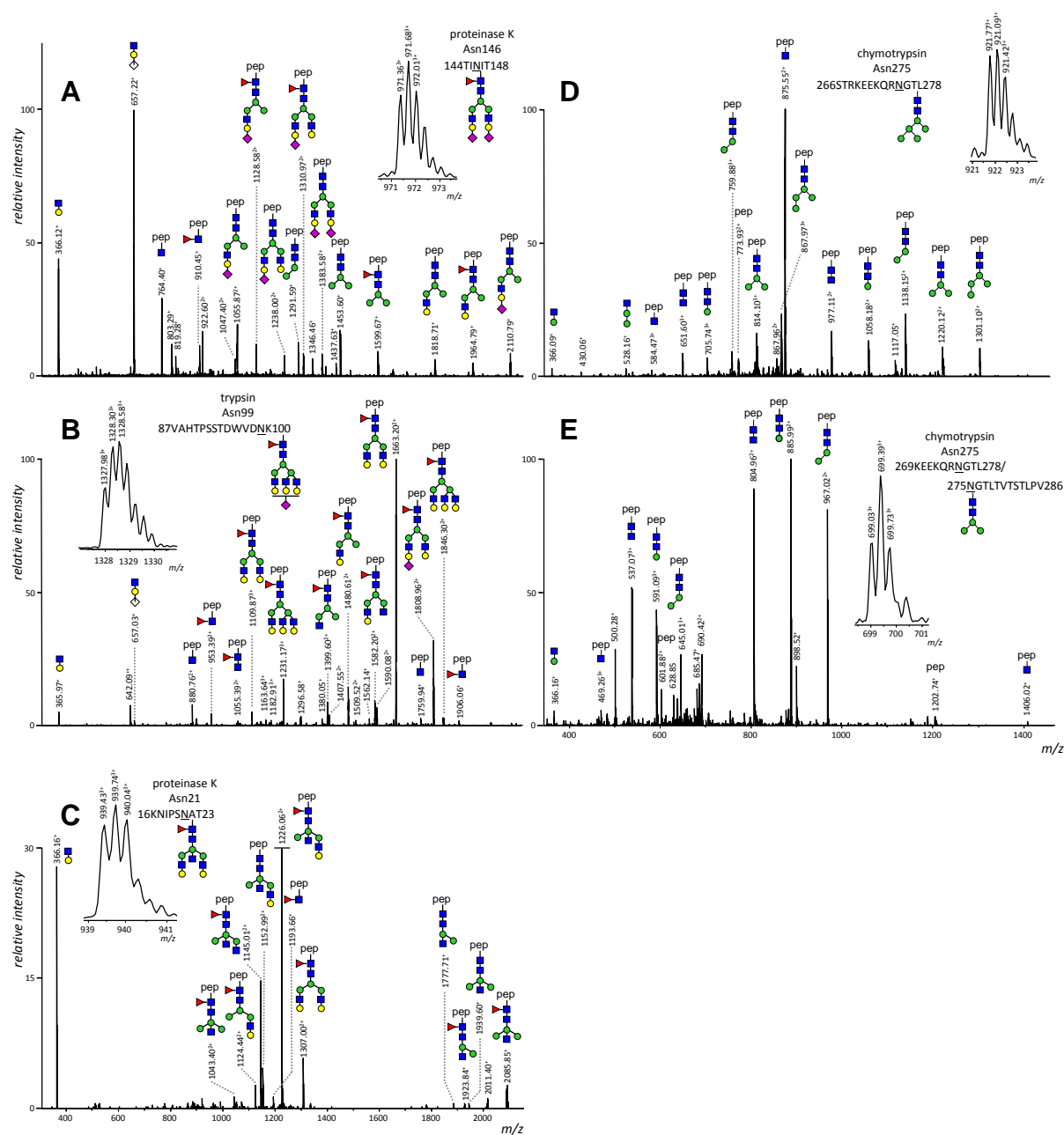
Figure 2.2: Fragmentation spectra obtained by nano-RP-LC-ESI-IT-MS/MS analysis of A) a proteinase K-generated glycopeptide from hyperimmune-IgE consisting of oligosaccharide structure H5N4S2F1 attached to peptide 144TINIT148; B) a trypsin-generated glycopeptide from myeloma-IgE consisting of H6N5S1F1 attached to 87VAHTPSSTDWVDNK100; C) a proteinase K-generated glycopeptide from hyperimmune-IgE consisting of H5N5F1 attached to 16KNIPSNAT23; D) a chymotrypsin-generated glycopeptide from hyperimmune-IgE consisting of H5N2 attached to 266STRKEEKQRNGTL278; and E) a chymotrypsin-generated glycopeptide from myeloma-IgE consisting of H3N2 attached to 269KEEKQRNGTL278/275NGTLTVTSTLPV286. H = hexose; N = *N*-acetylglucosamine; S = *N*-acetylneuraminic acid; F = fucose; pep = peptide; green circle = mannose; yellow circle = galactose; blue square = *N*-acetylglucosamine; red triangle = fucose; purple diamond = *N*-acetylneuraminic acid.

Figure 2.2C displays a proteinase K-generated glycopeptide covering Asn21 which contains a putative bisecting GlcNAc (an *N*-acetylglucosamine which is β1–4 linked to the innermost mannose). In order to confirm that this was indeed a bisected structure, glycans released from hyperimmune-IgE were labeled with 2-aminobenzoic acid (AA) and then characterized using both LC-MS/MS and UHPLC with fluorescence detection. LC-ESI-IT-MS/MS analysis showed an AA-labeled, protonated fragment consisting of 3 GlcNAc residues, 1 fucose and 1 hexose (*m/z* 1057.53) in the fragmentation spectrum of H5N5F1, indicating the presence of a bisecting GlcNAc (Supplemental Figure S2.2). Furthermore, UHPLC analysis of AA-labeled IgE glycans and AA-labeled IVIg glycans shows that the putative bisected structures in IgE elute at the same time as the corresponding structures of human intravenous immunoglobulin (IVIg; polyclonal human IgG), which have previously been shown to be bisected (Supplemental Figure S2.3) (25, 26). Moreover, if these structures were not bisected but instead contained a non-galactosylated third antenna, we would have expected to see non-galactosylated biantennary structures as well, which was not the case.

Oligomannosidic glycans were found on Asn275. The structure with 5 mannoses, exemplified by the MS/MS spectrum of a chymotrypsin-generated glycopeptide (Figure 2.2D), was the most prevalent. Furthermore, paucimannosidic glycans with 4 mannoses were present in all three types of IgE, and structures with 3 or 2 mannoses were found in myeloma-IgE and hyperimmune-IgE (Figure 2.2E). The MS/MS spectra of the oligomannosidic glycopeptides showed intense signals for [peptide + GlcNAc + H]$^+$, and MS3 analysis of this ion was used in some instances to confirm the peptide sequence (Supplemental Figure S2.4).
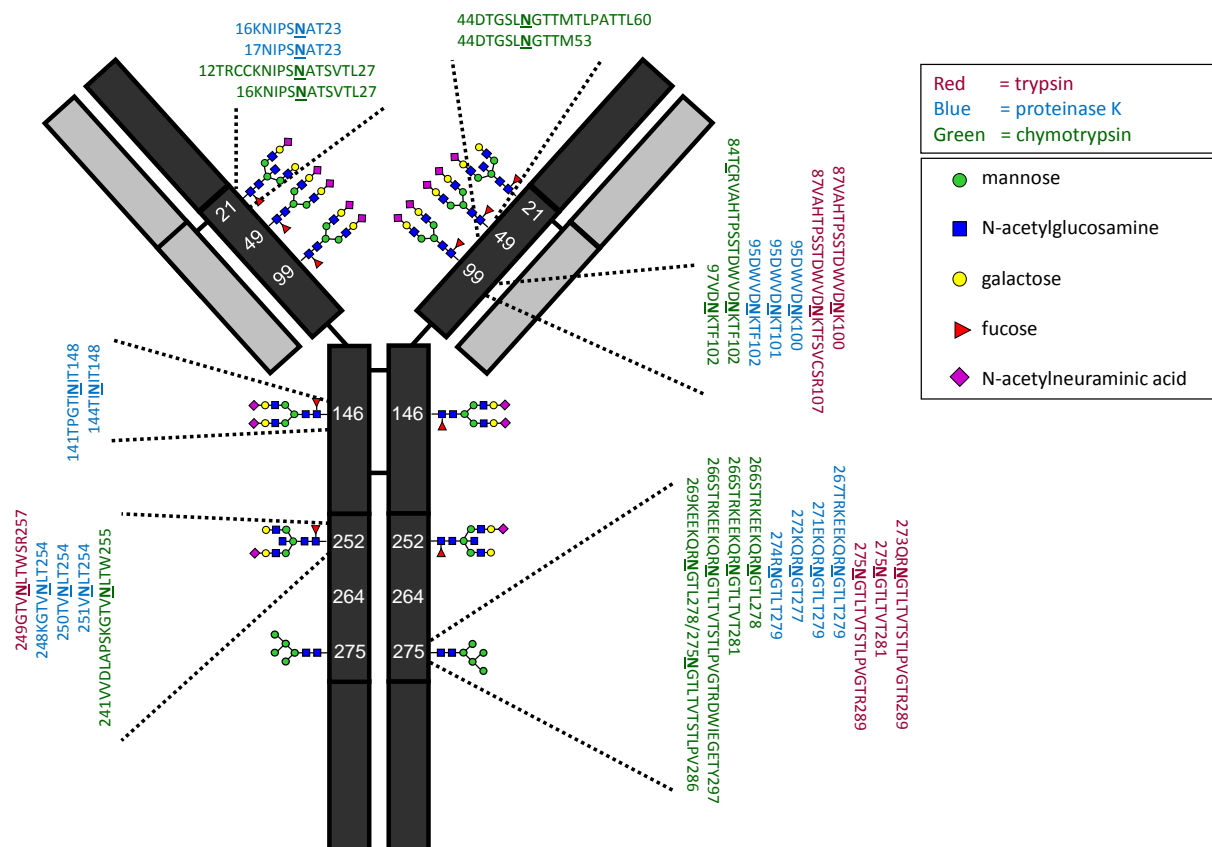
Figure 2.3: A model of IgE, which consists of 2 heavy chains (dark grey) and 2 light chains (light grey). Black lines connecting the chains represent disulfide bonds. Seven potential *N*-glycosylation sites are indicated by their amino acid residue number, and the most common oligosaccharide structure present at each site in IgE from healthy donors (as found by this study) is shown. For each occupied *N*-glycosylation site, several peptide sequences are shown which were observed during digestion with trypsin (shown in red), proteinase K (blue) or chymotrypsin (green).

Overall (Supplemental Figure S2.5), trypsin digestion allowed detection of glycopeptides covering Asn99, Asn252 and Asn275. Using proteinase K, glycopeptides covering Asn21, Asn99, Asn146, Asn252 and Asn275 were observed, while chymotrypsin allowed the analysis of glycans at Asn21, Asn49, Asn99, Asn252 and Asn275. The peptide sequences covered by each of these enzymes are listed in Figure 2.3, along with a scheme of the structure of IgE and its seven potential *N*-glycosylation sites. *N*-glycosylation sites Asn21, Asn49, Asn99, Asn146 and Asn252 were found to be occupied solely by complex-type carbohydrate structures in each of the three types of IgE. The vast majority of complex-type IgE glycan structures were found to contain a core fucose residue. Galactose residues were present on all antennae of complex-type glycans, and most structures also contained one or two terminal *N*-acetylneuraminic acid residues. Structures with a varying number of *N*-acetylneuraminic acids eluted at different time points, as can be seen in the extracted ion

chromatograms (EICs) of the glycopeptides containing Asn99 shown in Figure 2.4. The number of mannose residues present in the oligomannosidic glycan on Asn275 ranged from 2 to 9 mannoses, and all of these structures eluted at roughly the same time (Figure 2.5). To demonstrate the accuracy of our measurements, a comprehensive overview of all glycan species found in hyperimmune-IgE can be seen in Supplemental Table S2.2, along with the corresponding mass measurements and elution times.
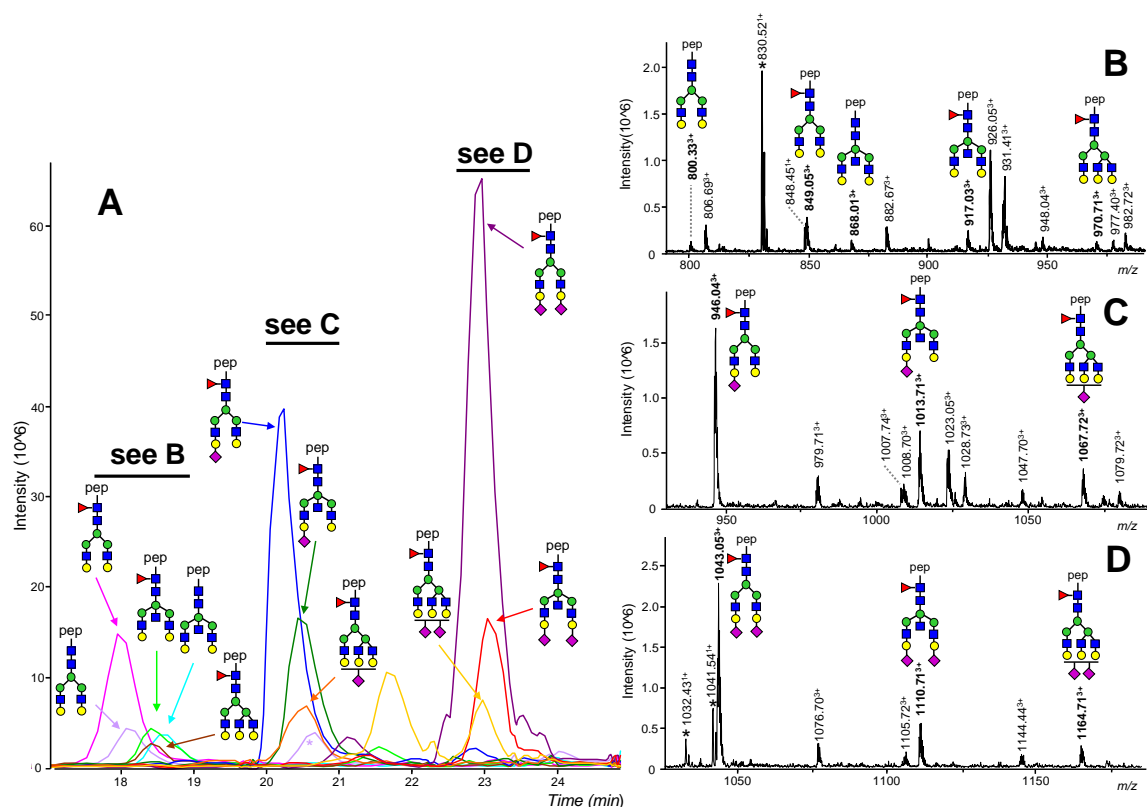
Figure 2.4: NanoLC-ESI-MS of a proteinase K digest of IgE derived from the serum of a single hyperimmune donor. A) Extracted ion chromatogram of the sum of the intensities of MS1 peaks of $[M+2H]^{2+}$ and $[M+3H]^{3+}$ species of glycopeptides corresponding to peptide 95DWVDNK100. Spectra are shown with annotated peaks for neutral glycan species (B), monosialylated glycans (C) and disialylated glycans (D). Peaks which belong to glycopeptides containing the peptide 95DWVDNK100 are shown in bold print; peaks that have been shown not to correspond to glycopeptides are marked with an asterisk. Green circle = mannose; yellow circle = galactose; blue square = *N*-acetylglucosamine; red triangle = fucose; purple diamond = *N*-acetylneuraminic acid; pep = peptide.
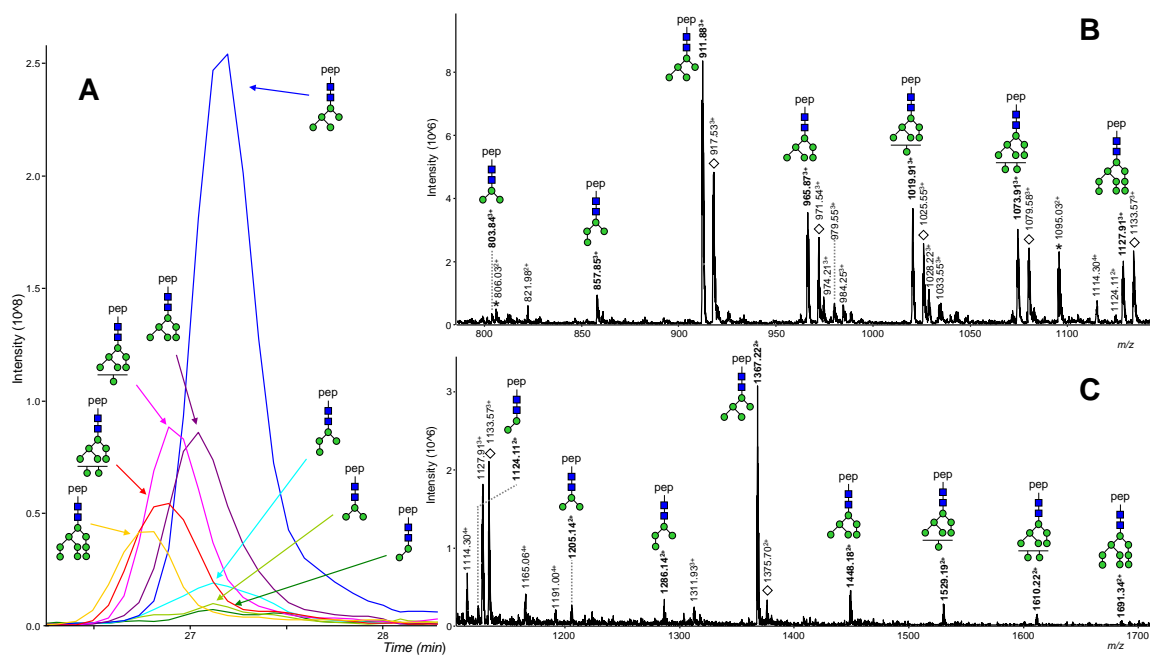
Figure 2.5: NanoLC-ESI-MS of a trypsin digest of IgE derived from the serum of a single hyperimmune donor. A) Extracted ion chromatogram of the sum of the intensities of peaks of [M+2H]2+ and [M+3H]3+ species of glycopeptides corresponding to peptide 275NGTLTVTSTLPVGTR289. Spectra with annotated [M+3H]3+ peaks (B) and [M+2H]2+ peaks (C) are shown. Modified glycopeptides containing an ammonia adduct are present, and are signified by a transparent diamond. Peaks which belong to unmodified glycopeptides containing the peptide 95DWVDNK100 are shown in bold print; peaks that have been shown not to correspond to glycopeptides are marked with an asterisk. Green circle = mannose; yellow circle = galactose; blue square = *N*-acetylglucosamine; red triangle = fucose; purple diamond = *N*-acetylneuraminic acid; pep = peptide.

Relative quantification of the glycan structures at each site was performed by summing the intensity of *m/z* values over a fixed time window around the elution time of each glycopeptide, and determining the background-corrected average intensity of the two highest isotopic peaks. This value was determined for each glycoform (if present in multiple charge states, the intensities of all charge states were summed) and normalized against the total of all glycoforms containing the same peptide moiety. The relative quantification profiles gathered from multiple digest samples were averaged for each glycosylation site, thus combining information from glycopeptides with different peptide moieties. Fortunately, the influence of the variation of the peptide moiety on the quantification profile appeared to be limited. This is illustrated by Supplemental Figure S2.6, which shows 17 relative quantification profiles acquired for site Asn99 in hyperimmune-IgE, based on glycopeptides with 7 different peptide moieties generated by either trypsin, proteinase K or chymotrypsin. The average relative quantification profile and the corresponding standard deviation of each of the six occupied *N*-

glycosylation sites was calculated separately for all three types of IgE, and is shown in the form of bar graphs (Figure 2.6). The number of separate profiles on which each average was based ranged from 2 to 17 (indicated in the inserts). The overall abundance of several *N*-glycosylation features (e.g. core fucose, bisecting GlcNAc, number of antennae, and the number of *N*-acetylneuraminic acids per galactose residue) is presented for each of the sites containing complex-type glycan structures (Figure 2.6, right part and Supplemental Table S2.3).
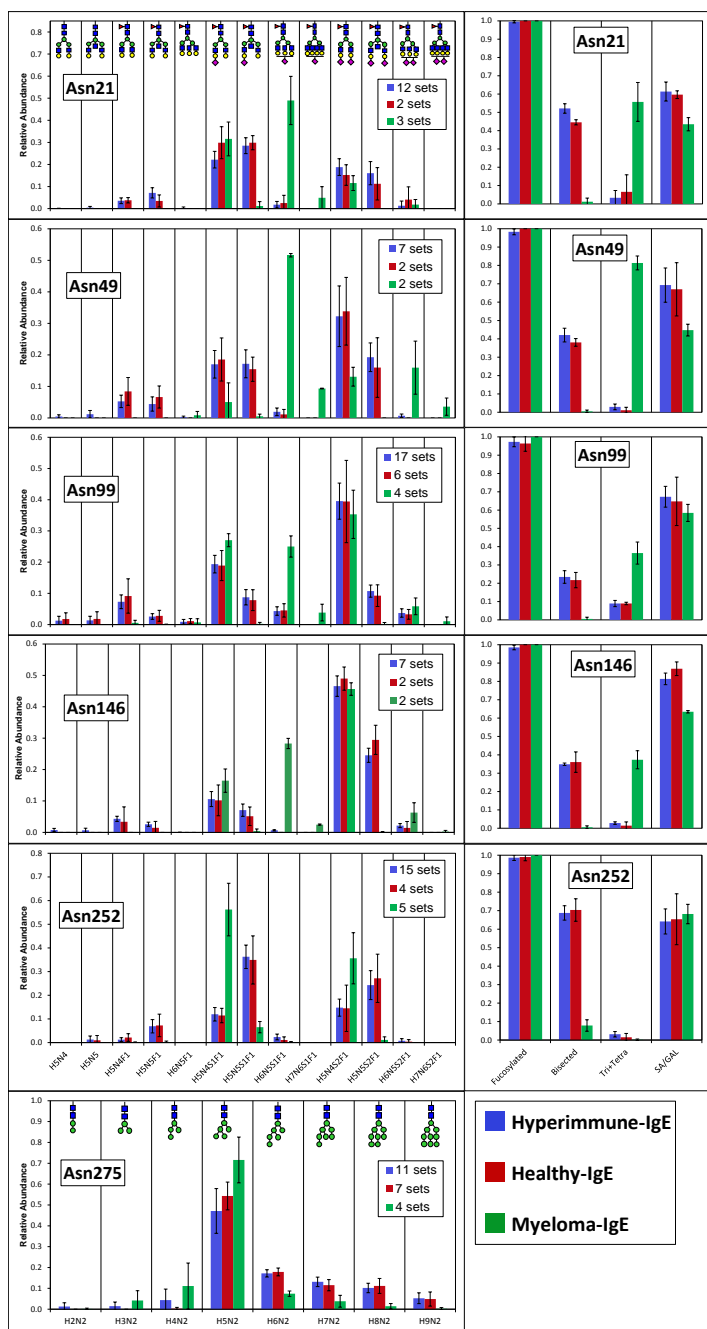
Figure 2.6: Glycosylation profiles of the 6 IgE *N*-glycosylation sites. Peak intensities were normalized to total intensity per glycosylation site, and averages and standard deviations are given based on multiple analyses with different enzymes as detailed in Supplemental Table S2.6. The number written behind the IgE type refers to the number of glycopeptide sets (with one glycopeptide set consisting of various glycoforms on one peptide from a separate enzymatic digest) which were used to calculate the average relative abundance. The complex-type glycosylation sites have an adjacent graph which outlines the following glycosylation features: fucosylation, incidence of bisecting *N*-acetylglucosamine, the number of *N*-acetylneuraminic acids per galactoses and the total percentage of triantennary and tetraantennary glycans. H = hexose; N = *N*-acetylglucosamine; S = *N*-acetylneuraminic acid; F = fucose; green circle = mannose; yellow circle = galactose; blue square = *N*-acetylglucosamine; red triangle = fucose; purple diamond = *N*-acetylneuraminic acid.

Low levels of non-fucosylated structures were observed in hyperimmune-IgE and healthy-IgE, whereas in myeloma-IgE all complex-type glycans were found to contain a core fucose. In all three types of IgE, the majority of complex-type glycans contained one or two terminal *N*-acetylneuraminic acid residues. Structures without *N*-acetylneuraminic acid were present at all five glycosylation sites which contain complex-type glycans in healthy-IgE and hyperimmune-IgE, while they were found only at sites Asn99 and Asn275, at very low levels, in the myeloma-IgE sample. In healthy- and hyperimmune-IgE, roughly 96% of complex-type glycan structures were found to be biantennary, while the remainder was triantennary. The myeloma-IgE sample was characterized by elevated levels of triantennary glycans (37%) and the presence of tetra-antennary structures (5%), at sites Asn21, Asn49, Asn99 and Asn146. Interestingly, at Asn252 myeloma-IgE does not contain tetra-antennary glycan structures, and the level of triantennary glycan structures at this site is actually lower for myeloma-IgE than for healthy- and hyperimmune-IgE. At most *N*-glycosylation sites, bisected glycans form a minority. The exception is formed by site Asn252, where bisected glycan structures are more abundant than non-bisected glycans in healthy-IgE and hyperimmune-IgE. In myeloma-IgE, the level of bisected glycan structures is substantially lower: less than 1.5% of all glycans at Asn21, Asn49, Asn99 and Asn146 and approx. 8% at Asn252.

The potential *N*-glycosylation site Asn264 was not covered by any peptide in the LC-MS/MS results of the proteolytic digests. It was suspected that this was due to the hydrophilicity of the amino acid sequence surrounding this site. This was confirmed by LC-MS/MS analysis of the synthetically produced peptide 258ASGKPVNHSTR268, corresponding to the *in silico* tryptic peptide covering this potential glycosylation site. When this sample was analyzed by LC-MS/MS in the same way as the enzymatic digests, which includes trapping and washing of a pre-column, the peptide was not found. However, by disabling the pre-column and bringing the sample directly onto the nano-column, this peptide was observed in the flow-through (data not shown). Therefore, MALDI-TOF-MS analysis seemed more appropriate to study potential glycosylation at this site. For this purpose, we analyzed tryptic digests of myeloma-IgE and hyperimmune-IgE before and after treatment with *N*-glycosidase F. Both samples displayed a near-identical isotope distribution (shown in Supplemental Figure S2.7 for myeloma-IgE), demonstrating that the apparent partial deamidation was spontaneous and that Asn264 is not occupied by carbohydrate structures.

The sites Asn99, Asn252 and Asn275 were found to be partially unoccupied, as peptides covering these sites were observed in proteolytic digests without *N*-glycosidase F treatment (Supplemental Figure S2.5). This was confirmed by the fact that the unoccupied tryptic peptides 87VAHTPSSTDWVD**N**K100, 249GTV**N**LTWSR257 and 275**D**GTLTVTSTLPVGTR289 (the last one being present only in deamidated form, as has been shown to be characteristic for Asn-Gly sequences (27)) were found in ESI-LC-IT-MS(/MS) and MALDI-TOF(/TOF)-MS/MS analysis of both *N*-glycosidase F-treated and non-*N*-glycosidase F-treated IgE. To calculate the degree of site occupancy, two methods were used.

The first method involved determination of the ratio of deamidated vs. unmodified peptide from the isotope distribution in an *N*-glycosidase F-treated sample. This was corrected for spontaneous deamidation if this was observed in a non-N glycosidase-treated sample which was incubated likewise.

The second method relied on performing relative quantification of both glycopeptides and the corresponding unoccupied peptide from LC-MS data of a non-*N*-glycosidase F-treated sample. Notably, these methods produced comparable results. The degree of occupation (% of peptides occupied by glycans±standard deviation) of Asn99, Asn252 and Asn275 was found to be 80±7% (range: 65-86%), 96±2% (range: 92-98%) and 98±3% (range: 92-100%), respectively, in both hyperimmune- and myeloma-IgE (Supplemental Table S2.4).

2.5: Discussion

In this paper we used a combination of various enzymatic digestions and nano-RP-LC-ESI-IT- and MALDI-TOF/TOF-MS/MS to study site-specific glycosylation in polyclonal immunoglobulin E derived from various sources. Previously, site-specific analysis of the glycosylation of IgE has only been performed on monoclonal myeloma-derived protein using gas-liquid chromatography or on recombinant IgE (7, 16-18). None of these studies have investigated all seven potential IgE *N*-glycosylation sites. We found that by combining the data from proteinase K and chymotrypsin digestion, all 6 occupied *N*-glycosylation sites in the conserved region of the heavy chain can be explored. We confirmed the presence of complex-type *N*-glycosylation structures at Asn21, Asn49, Asn99, Asn146 and Asn252 and oligomannosidic structures at Asn275, in all three types of polyclonal IgE. In accordance with literature, potential *N*-glycosylation site Asn264 was found not to be occupied by *N*-glycans; Asn99, Asn252 and Asn275 were shown to be only partially occupied.

To evaluate the performance of our method in studying site-specific IgE glycosylation profiles and the differences in IgE glycosylation under different physiological conditions, we chose to include a myeloma-derived IgE sample. As expected, the glycosylation profile of the myeloma-IgE sample was found to be markedly different, while the glycosylation of the healthy-IgE and hyperimmune-IgE samples was found to be quite similar. Overall, the level of triantennary and tetraantennary complex-type glycan structures was greatly elevated in myeloma-IgE. Although the linkage types of the antennae within the glycan structures found in this study are not known, it is likely that the increase in tri- and tetraantennary complex-type structures in myeloma-IgE is due to an increase in β1-6-linked branching, which has been observed in previous studies for various types of cancer tissue (28, 29). Accordingly, we found the abundance of glycans with a bisecting *N*-acetylglucosamine to be severely decreased in myeloma-IgE, which is likewise a known glycosylation feature of malignancies (30). Furthermore, no non-fucosylated complex-type glycans were encountered in myeloma-IgE, and the level of complex-type structures which did not contain *N*-acetylneuraminic acids was found to be lower than in healthy-IgE and hyperimmune-IgE. It should be stressed that these results are based on 3 (pooled) samples. Therefore these findings should be considered as examples of how such profiles can be studied using our method, and not as conclusive in describing overall IgE glycosylation under these (patho)physiological conditions.

The validity of nanoLC-ESI-IT-MS for the determination of site occupancy is not undisputed. Recently, Stavenhagen *et al.* studied the influence of (glyco)peptide characteristics in glycoproteomic workflows on signal intensities and consequently on relative site occupancy with MS-based techniques (31). Using a limited set of structurally related (glyco)peptides, they observed lower signal strength of both di- and non-sialylated biantennary *N*-glycopeptides as compared to the non-glycosylated counterparts. Moreover, they observed a slight reduction in intensity upon Asn-Asp exchange (analogous to PNGase F treatment), especially when the aspartic acid was close to the C-terminus of the (tryptic-like) peptide. These ion suppression effects were to a large extent dependent on the ionization source, with nano-ESI allowing to avoid the ionization suppression to a large extent. With regard to our determination of site occupancies, these results imply that comparing signal strengths of glycopeptides and peptides without any correction factor will most likely result in underestimation of the glycopeptide relative abundance and consequently the site-occupancy. Likewise, direct comparison of peptides with a potential *N*-glycosylation site containing the Asn or Asp (generated by PNGase treatment and/or spontaeous deamidation) may result in slightly biased site occupancies. In view of these considerations, it is remarkable that the site occupancies determined in our study by different approaches show a rather good agreement. In addition, the fact that disialylated glycopeptides were reported to generate a lower signal than corresponding non-sialylated species indicates that the level of sialylation found in our study might be somewhat lower than the real values (31).

The type of glycans (complex or oligomannosidic) present at each IgE *N*-glycosylation site as determined by our study matches the findings of previous studies (7, 17, 18). However, this comparison is complicated by the fact that the two previous site-specific IgE characterization studies were performed solely on monoclonal, myeloma-derived IgE, and by the fact that these studies determined only the relative abundance of monosaccharide residues, and not the actual glycan structures (7, 17, 18). These findings do not always correspond with our data. For example, Dorrington *et al.* reported only trace amounts of fucose at Asn99 and Asn146, while our findings show the majority of glycans at these sites to be fucosylated in all three IgE samples (7). A study by Arnold *et al.* on released glycan structures of the IgE heavy chain derived from the serum of a hyperimmune donor also shows several markedly different results (20). Contrary to our findings, they reported no tri- and tetraantennary structures, but they did encounter four different monoantennary glycans and one hybrid-type glycan.

Furthermore, they report that approx. 68% of complex-type IgE glycans contained a core fucose, while the degree of fucosylation in the three samples we analyzed was found to lie between 98.5% and 100%.

Heavy chain glycosylation of several other members of the immunoglobulin family has been shown to influence protein solubility, transport and lectin- and receptor-binding (32, 33). Sequence alignment revealed the IgE *N*-glycosylation site Asn275 to be homologous to Asn297 in IgG, Asn364 in IgD and Asn402 in IgM, indicating functional significance. While Asn275 is occupied by complex-type *N*-glycans in IgG, the homologous sites in IgE, IgD and IgM contain oligomannosidic glycan structures (33). Removal of Asn297 in IgG has been shown to affect thermodynamic stability and receptor binding (34). Further evidence for functional significance of Asn275 emerges from the discovery that, while mutation of potential *N*-glycosylation sites Asn252 or Asn264 (N➜Q) did not influence IgE-FcεRI interaction, mutation of Asn275 or Thr277 resulted in loss of binding (16). However, this loss of binding was also observed when the oligosaccharide occupation of Asn275 was not affected (T277➜S mutation). In general, glycosylation is thought to make only a minor or no contribution to FcεRI binding (11-13), although one account of a severe loss in binding after deglycosylation of IgE has been described (10). Moreover, glycosylation of IgE has been shown to affect binding affinity for CD23 (13). It has been theorized that the presence of glycans at Asn252 could directly affect the interaction between IgE and CD23 (35). The immune regulators galectin-3 and galectin-9 also bind to IgE in a glycosylation-dependent manner, and it is speculated that galectin-IgE binding has a negative effect on IgE-antigen and IgE-receptor binding (14, 36). These are only a few of the ways by which glycosylation of IgE can influence its activity, and more functional research is needed to further elucidate the biological role of IgE glycosylation.

Due to their association with adverse or protective IgE responses, allergy and parasitic diseases are favorable candidates for further studies (5, 6). While this study has uncovered no significant differences between the IgE glycosylation profile of a single hyperimmune donor and that of healthy individuals, it will be interesting to examine if this similarity holds true when comparing large numbers of individuals with various allergic conditions.

In conclusion, this study describes a comprehensive overview of the glycosylation of polyclonal IgE and provides a workflow of how this can be studied in a site-specific manner.

Our aim is to further develop our method in order to determine disease-associated glycosylation changes of IgE. This is motivated by the fact that IgE glycosylation has been known to show inter-individual variation (21) and has been implicated in modulating biological activity. To this end, we are currently working on setting up a robust method for IgE purification from serum, which shall be combined with ultrahigh-sensitivity analysis of glycopeptides (37) in order to comply with the often limited amounts of IgE that can be obtained from serum or plasma samples (1-3).

References

1.   King, C. L., Poindexter, R. W., Ragunathan, J., Fleisher, T. A., Ottesen, E. A., and Nutman, T. B. (1991) Frequency analysis of IgE-secreting B lymphocytes in persons with normal or elevated serum IgE levels. *J Immunol* 146, 1478-1483

2.   Ghory, A. C., Patterson, R., Roberts, M., and Suszko, I. (1980) In vitro IgE formation by peripheral blood lymphocytes from normal individuals and patients with allergic bronchopulmonary aspergillosis. *Clin Exp Immunol* 40, 581-585

3.   Johansson, S. G. (1967) Raised levels of a new immunoglobulin class (IgND) in asthma. *Lancet* 2, 951-953

4.   Wan, T., Beavil, R. L., Fabiane, S. M., Beavil, A. J., Sohi, M. K., Keown, M., Young, R. J., Henry, A. J., Owens, R. J., Gould, H. J., and Sutton, B. J. (2002) The crystal structure of IgE Fc reveals an asymmetrically bent conformation. *Nat Immunol* 3, 681-686

5.   Gounni, A. S., Lamkhioued, B., Ochiai, K., Tanaka, Y., Delaporte, E., Capron, A., Kinet, J. P., and Capron, M. (1994) High-affinity IgE receptor on eosinophils is involved in defence against parasites. *Nature* 367, 183-186

6.   Gould, H. J., and Sutton, B. J. (2008) IgE in allergy and asthma today. *Nat Rev Immunol* 8, 205-217

7.   Dorrington, K. J., and Bennich, H. H. (1978) Structure-function relationships in human immunoglobulin E. *Immunol Rev* 41, 3-25

8.   Granato, D. A., and Neeser, J. R. (1987) Effect of trimming inhibitors on the secretion and biological activity of a murine IgE monoclonal antibody. *Mol Immunol* 24, 849-855

9.   Platzer, B., Ruiter, F., van der Mee, J., and Fiebiger, E. (2011) Soluble IgE receptors--elements of the IgE network. *Immunol Lett* 141, 36-44

10.   Bjorklund, J. E., Karlsson, T., and Magnusson, C. G. (1999) N-glycosylation influences epitope expression and receptor binding structures in human IgE. *Mol Immunol* 36, 213-221

11.   Woof, J. M., and Burton, D. R. (2004) Human antibody-Fc receptor interactions illuminated by crystal structures. *Nat Rev Immunol* 4, 89-99

12.   Basu, M., Hakimi, J., Dharm, E., Kondas, J. A., Tsien, W. H., Pilson, R. S., Lin, P., Gilfillan, A., Haring, P., Braswell, E. H., and et al. (1993) Purification and characterization of human recombinant IgE-Fc fragments that bind to the human high affinity IgE receptor. *J Biol Chem* 268, 13118-13127

13.   Vercelli, D., Helm, B., Marsh, P., Padlan, E., Geha, R., and Gould, H. (1989) The B-cell binding site on human immunoglobulin E. *Nature* 338, 649-651

14.   Frigeri, L. G., Zuberi, R. I., and Liu, F. T. (1993) Epsilon BP, a beta-galactoside-binding animal lectin, recognizes IgE receptor (Fc epsilon RI) and activates mast cells. *Biochemistry* 32, 7644-7649

15.   Niki, T., Tsutsui, S., Hirose, S., Aradono, S., Sugimoto, Y., Takeshita, K., Nishi, N., and Hirashima, M. (2009) Galectin-9 Is a High Affinity IgE-binding Lectin with Anti-allergic Effect by Blocking IgE-Antigen Complex Formation. *Journal of Biological Chemistry* 284, 32344-32352

16.   Nettleton, M. Y., and Kochan, J. P. (1995) Role of glycosylation sites in the IgE Fc molecule. *Int Arch Allergy Immunol* 107, 328-329

17.   Baenziger, J., Kornfeld, S., and Kochwa, S. (1974) Structure of the Carbohydrate Units of IgE Immunoglobulin: II. Sequence of the Sialic Acid-containing Glycopeptides. *Journal of Biological Chemistry* 249, 1897-1903

18.   Baenziger, J., Kornfeld, S., and Kochwa, S. (1974) Structure of the Carbohydrate Units of IgE Immunoglobulin: I. Over-all Composition, Glycopeptide Isolation, and Structure of the High Mannose Oligosaccharide Unit. *Journal of Biological Chemistry* 249, 1889-1896

19.   Fridriksson, E. K., Beavil, A., Holowka, D., Gould, H. J., Baird, B., and McLafferty, F. W. (2000) Heterogeneous Glycosylation of Immunoglobulin E Constructs Characterized by Top-Down High-Resolution 2-D Mass Spectrometry†. *Biochemistry* 39, 3369-3376

20.   Arnold, J. N., Radcliffe, C. M., Wormald, M. R., Royle, L., Harvey, D. J., Crispin, M., Dwek, R. A., Sim, R. B., and Rudd, P. M. (2004) The Glycosylation of Human Serum IgD and IgE and the

Accessibility of Identified Oligomannose Structures for Interaction with Mannan-Binding Lectin. *The Journal of Immunology* 173, 6831-6840

21.   Robertson, M. W., and Liu, F. T. (1991) Heterogeneous IgE glycoforms characterized by differential recognition of an endogenous lectin (IgE-binding protein). *J Immunol* 147, 3024-3030

22.   Huddleston, M. J., Bean, M. F., and Carr, S. A. (1993) Collisional fragmentation of glycopeptides by electrospray ionization LC/MS and LC/MS/MS: methods for selective detection of glycopeptides in protein digests. *Anal Chem* 65, 877-884

23.   Sullivan, B., Addona, T. A., and Carr, S. A. (2004) Selective detection of glycopeptides on ion trap mass spectrometers. *Anal Chem* 76, 3112-3118

24.   Wuhrer, M., Catalina, M. I., Deelder, A. M., and Hokke, C. H. (2007) Glycoproteomics based on tandem mass spectrometry of glycopeptides. *J Chromatogr B Analyt Technol Biomed Life Sci* 849, 115-128

25.   Mizuochi, T., Taniguchi, T., Shimizu, A., and Kobata, A. (1982) Structural and numerical variations of the carbohydrate moiety of immunoglobulin G. *J Immunol* 129, 2016-2020

26.   Lauc, G., Huffman, J. E., Pucic, M., Zgaga, L., Adamczyk, B., Muzinic, A., Novokmet, M., Polasek, O., Gornik, O., Kristic, J., Keser, T., Vitart, V., Scheijen, B., Uh, H. W., Molokhia, M., Patrick, A. L., McKeigue, P., Kolcic, I., Lukic, I. K., Swann, O., van Leeuwen, F. N., Ruhaak, L. R., Houwing-Duistermaat, J. J., Slagboom, P. E., Beekman, M., de Craen, A. J., Deelder, A. M., Zeng, Q., Wang, W., Hastie, N. D., Gyllensten, U., Wilson, J. F., Wuhrer, M., Wright, A. F., Rudd, P. M., Hayward, C., Aulchenko, Y., Campbell, H., and Rudan, I. (2013) Loci associated with N-glycosylation of human immunoglobulin G show pleiotropy with autoimmune diseases and haematological cancers. *PLoS Genet* 9, e1003225

27.   Krokhin, O. V., Antonovici, M., Ens, W., Wilkins, J. A., and Standing, K. G. (2006) Deamidation of -Asn-Gly- sequences during sample preparation for proteomics: Consequences for MALDI and HPLC-MALDI analysis. *Anal Chem* 78, 6645-6650

28.   Dennis, J. W., Granovsky, M., and Warren, C. E. (1999) Glycoprotein glycosylation and cancer progression. *Biochim Biophys Acta* 1473, 21-34

29.   Kim, Y. J., and Varki, A. (1997) Perspectives on the significance of altered glycosylation of glycoproteins in cancer. *Glycoconj J* 14, 569-576

30.   Balog, C. I., Stavenhagen, K., Fung, W. L., Koeleman, C. A., McDonnell, L. A., Verhoeven, A., Mesker, W. E., Tollenaar, R. A., Deelder, A. M., and Wuhrer, M. (2012) N-glycosylation of colorectal cancer tissues: a liquid chromatography and mass spectrometry-based investigation. *Mol Cell Proteomics* 11, 571-585

31.   Stavenhagen, K., Hinneburg, H., Thaysen-Andersen, M., Hartmann, L., Varon Silva, D., Fuchser, J., Kaspar, S., Rapp, E., Seeberger, P. H., and Kolarich, D. (2013) Quantitative mapping of glycoprotein micro-heterogeneity and macro-heterogeneity: an evaluation of mass spectrometry signal strengths using synthetic peptides and glycopeptides. *J Mass Spectrom* 48, 627-639

32.   Ferrara, C., Grau, S., Jager, C., Sondermann, P., Brunker, P., Waldhauer, I., Hennig, M., Ruf, A., Rufer, A. C., Stihle, M., Umana, P., and Benz, J. (2011) Unique carbohydrate-carbohydrate interactions are required for high affinity binding between FcgammaRIII and antibodies lacking core fucose. *Proc Natl Acad Sci U S A* 108, 12669-12674

33.   Arnold, J. N., Wormald, M. R., Sim, R. B., Rudd, P. M., and Dwek, R. A. (2007) The impact of glycosylation on the biological function and structure of human immunoglobulins. *Annu Rev Immunol* 25, 21-50

34.   Jefferis, R., Lund, J., and Pound, J. D. (1998) IgG-Fc-mediated effector functions: molecular definition of interaction sites for effector ligands and the role of glycosylation. *Immunol Rev* 163, 59-76

35.   Sondermann, P., Pincetic, A., Maamary, J., Lammens, K., and Ravetch, J. V. (2013) General mechanism for modulating immunoglobulin effector function. *Proc Natl Acad Sci U S A* 110, 9868-9872

36.   Niki, T., Tsutsui, S., Hirose, S., Aradono, S., Sugimoto, Y., Takeshita, K., Nishi, N., and Hirashima, M. (2009) Galectin-9 is a high affinity IgE-binding lectin with anti-allergic effect by blocking IgE-antigen complex formation. *J Biol Chem* 284, 32344-32352

37.   Heemskerk, A. A., Wuhrer, M., Busnel, J. M., Koeleman, C. A., Selman, M. H., Vidarsson, G., Kapur, R., Schoenmaker, B., Derks, R. J., Deelder, A. M., and Mayboroda, O. A. (2013) Coupling porous sheathless interface MS with transient-ITP in neutral capillaries for improved sensitivity in glycopeptide analysis. *Electrophoresis* 34, 383-387

38.   Wuhrer, M., Koeleman, C. A., Hokke, C. H., and Deelder, A. M. (2006) Mass spectrometry of proton adducts of fucosylated N-glycans: fucose transfer between antennae gives rise to misleading fragments. *Rapid Commun Mass Spectrom* 20, 1747-1754

39.   Selman, M. H., Hemayatkar, M., Deelder, A. M., and Wuhrer, M. (2011) Cotton HILIC SPE microtips for microscale purification and enrichment of glycans and glycopeptides. *Anal Chem* 83, 2492-2499

Supplemental Information

A complete overview of the supplemental information is available online at http://pubs.acs.org/doi/suppl/10.1021/pr400714w.
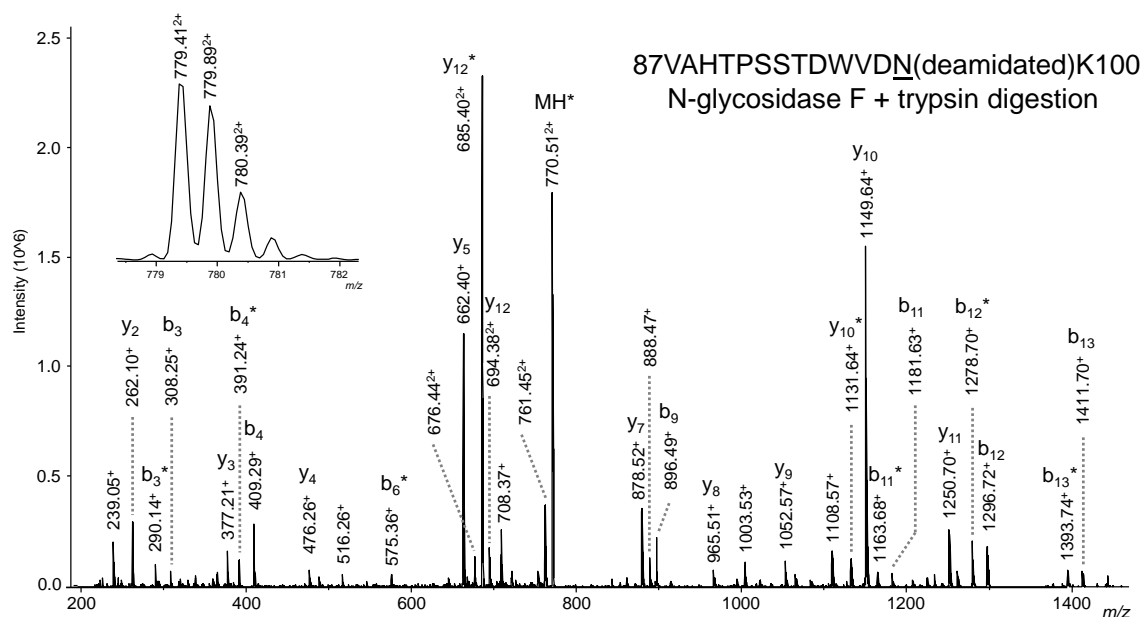

Supplemental Figure S2.1: MS/MS spectrum from LC-ESI-IT-MS analysis corresponding to the deamidated trypsin-generated peptide 87VAHTPSSTDWVDN(deamidated)K100 from myeloma-IgE. Glycan release with *N*-glycosidase F has been performed on the sample, followed by trypsin digestion. The *m/z* values of singly and doubly charged b and y fragment ions are given. Loss of water (-18 Da) is denoted by an asterisk.
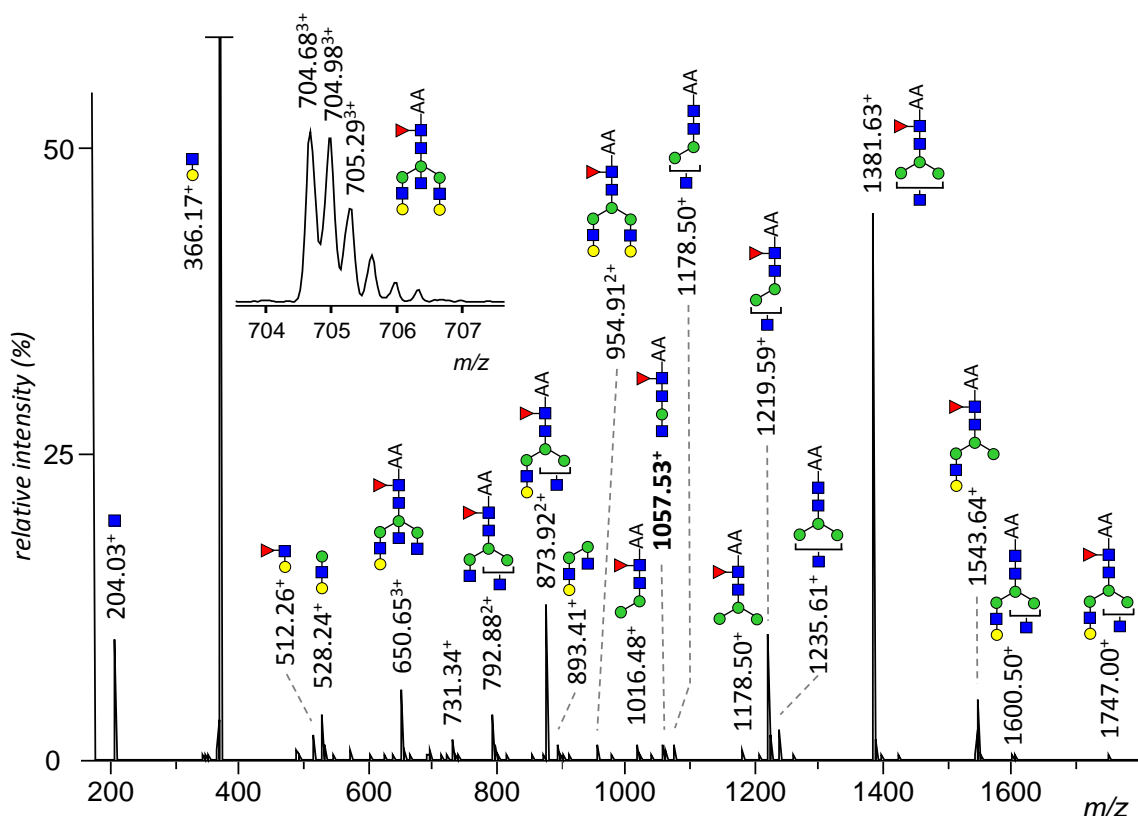
Supplemental Figure S2.2: MS/MS spectrum of the H5N5F1 structure from LC-ESI-IT-MS analysis of 2-aminobenzoic acid-labeled IgE glycans. The peak at *m/z* 1057.53 indicates that the glycan contains a bisecting *N*-acetylglucosamine. The peak at *m/z* 512.26 corresponds to [HexNAc + hexose + fucose + H]$^+$, but this structure is most likely due to fucose migration, as described previously (38). Green circle = mannose; yellow circle = galactose; blue square = *N*-acetylglucosamine; red triangle = fucose; AA = 2-aminobenzoic acid.

For in-solution glycan release, 10 µg of hyperimmune-IgE in 20 µl 1.3%SDS Milli-Q-purified water was first incubated at 60°C for 10 min. Next, 10µl of 2% Tergitol type NP-40, 10 µl of 5xPBS and 1 µl of *N*-glycosidase F (1 unit) were added, and glycan release was performed overnight at 37°C. An AA-label was introduced by adding 15 µl labeling solution (48mg/ml AA in 85%DMSO 15% acetic acid) and 15µl reducing solution (107mg/ml 2-picoline borane in DMSO). The sample was vortexed thoroughly, and incubated at 65°C for 2 h. The glycans were then purified using cotton HILIC SPE, as described by Selman *et al.* (39) The cotton tip was first equilibriated 3x with water and 3x with 85% acetonitrile (ACN). The sample with labeled glycans was brought to 85% ACN and run through the cotton tip around 40x. The cotton tip was then washed 3x with 85% ACN 1% trifluoroacetic acid and 3x with 85% ACN, before the glycans were eluted in 10 µl Milli-Q-purified water.
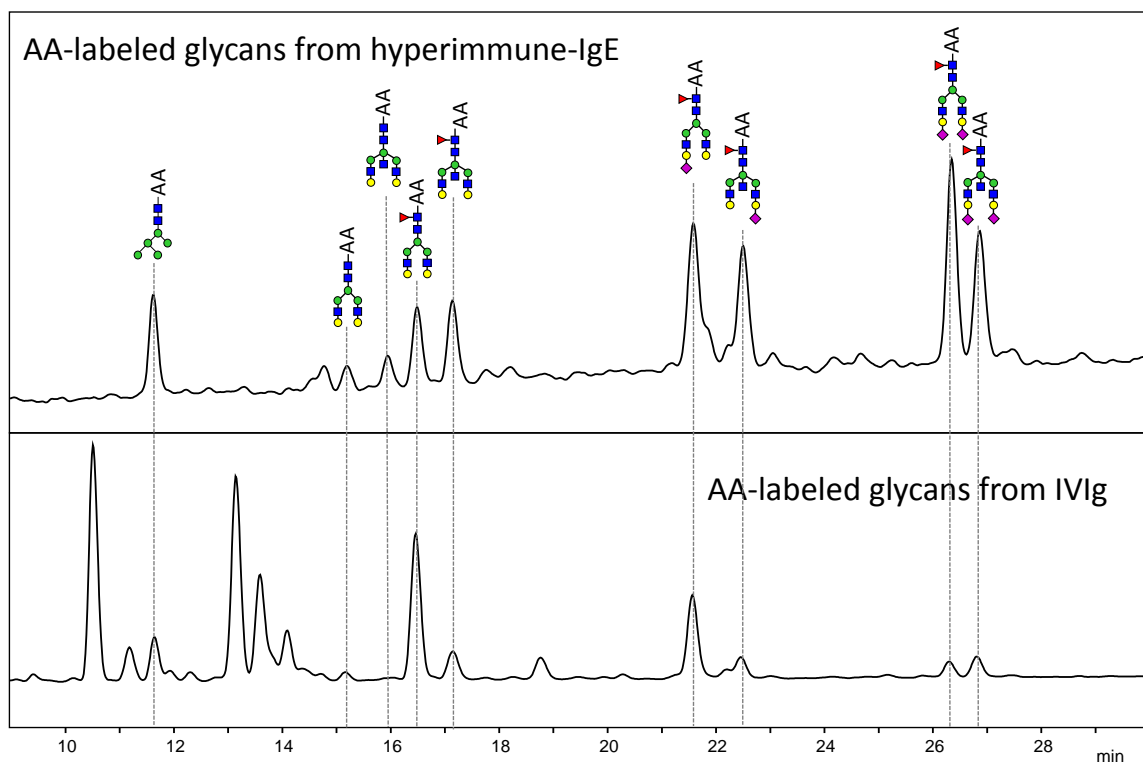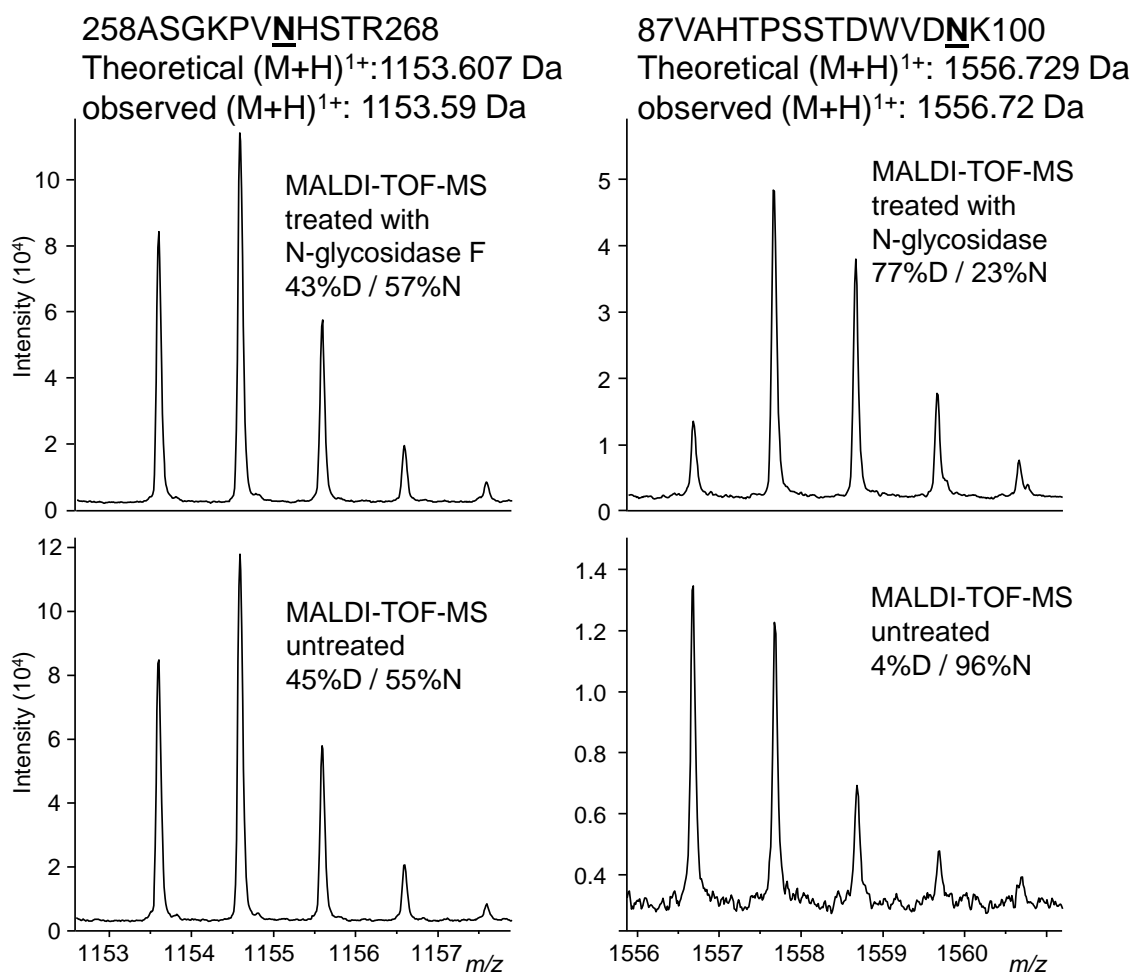
Supplemental Figure S2.3: UHPLC analysis of 2-aminobenzoic acid (AA)-labeled glycans from hyperimmune-IgE and from human IVIg (Nanogam).

Glycan release, labeling and purification were performed as described under Supplemental Figure S2.2. The samples were analyzed on a Dionex Ultimate 3000 UHPLC system, coupled to an FLD-3400RS fluorescence detector (Dionex/Thermo Scientific). Separation was achieved on an AQUITY UPLC BEH Glycan column (2.1 x 100mm, particle size 1.7 µm, Waters), with a flow of 0.6 ml/min and an oven temperature of 60°C. Solvent A consisted of 100 mM ammonium formate in water; solvent B of acetonitrile. A linear gradient was applied with the following conditions: t=0 min, 15% solvent A; t=0.5 min, 15% solvent A; t=0.5 min, 25% solvent A; t=45.5 min; 43% solvent A; t=45.5 min, 60% solvent A; t=49.5 min, 60% solvent A; t=49.5 min, 15% solvent A.

The 2-AA labeled glycans of IgE were identified based on the comparison of their HPLC elution patterns with those of fluorescently labeled IgG *N*-glycans previously described by Lauc *et al.* (26) The H5N5F1, H5N5S1F1 and H5N5S2F1 structures were confirmed by LC-ESI-IT-MS/MS analysis of UHPLC fractions. Green circle = mannose; yellow circle = galactose; blue square = *N*-acetylglucosamine; red triangle = fucose; purple diamond = *N*-acetylneuraminic acid; AA = 2-aminobenzoic acid.

258ASGKPV**N**HSTR268
Theoretical (M+H)$^{1+}$:1153.607 Da
observed (M+H)$^{1+}$: 1153.59 Da

87VAHTPSSTDWVD**N**K100
Theoretical (M+H)$^{1+}$: 1556.729 Da
observed (M+H)$^{1+}$: 1556.72 Da

MALDI-TOF-MS
treated with
N-glycosidase F
43%D / 57%N

MALDI-TOF-MS
treated with
N-glycosidase
77%D / 23%N

MALDI-TOF-MS
untreated
45%D / 55%N

MALDI-TOF-MS
untreated
4%D / 96%N

Supplemental Figure S2.7: MALDI-TOF-MS spectra of both a deglycosylated and an untreated trypsin digest of myeloma-IgE. Before trypsin digestion was performed, one of the digests was treated with *N*-glycosidase F, while the other was incubated in buffer. This was done to observe the degree of spontaneous deamidation. The two spectra on the left show the isotope distribution corresponding to a peptide containing the potential *N*-glycosylation site Asn264; the spectra on the right correspond to a peptide containing glycosylation site Asn99. The ratio of deaminated ('D') peptide versus non-deaminated ('N') peptide was determined from the theoretical isotope distribution. Peptide sequences were confirmed with MALDI-TOF/TOF-MS.